# Supplementary Information

## Burger, Li, Keating, Sivina, Amer et al:

# "Leukemia cell proliferation and death in CLL patients on ibrutinib therapy"

**CONTENTS**

***Cell staining, separation, and measurement of isotopic enrichment in CLL-cell DNA***

PBMC were isolated from 50 ml of heparinized fresh blood by Ficoll-Paque (GE Healthcare, Piscataway, NJ, USA) density gradient centrifugation. $CD3^+$ T cells were removed from these fractions by positive selection using anti-CD3 microbeads (Miltenyi Biotec, Inc.) following the manufacturer's instructions. $CD5^+$ B cells were separated from the $CD3^-$ fraction by incubation with anti-CD5 mAb conjugated with PE (BD Biosciences Immunocytometry Systems) for 20 minutes at 4°C, washing 4 times in buffer (PBS, 5% BSA, 2 mM EDTA), and subsequent incubation with anti-PE mAb linked to beads (Miltenyi Biotec Inc.). The $CD5^+$ fraction, which contained greater than 95% $CD19^+$ cells as assessed by flow cytometry, was centrifuged into a pellet and stored frozen at –20°C until further use. The enrichment of $^2H_2O$ in plasma was measured by gas chromatography/mass spectrometry (GC/MS) as described previously(*1*). $^2H_2O$ enrichment was calculated by comparison with standard curves generated by mixture of 100% $^2H_2O$ with natural-abundance $H_2O$ in known proportions.

***Measurement of isotopic enrichment in CLL-cell DNA***

Isotope enrichment in CLL-cell DNA was analyzed as described(*2*). Briefly, DNA was isolated from CLL B cells and hydrolyzed to free nucleosides. Isotopic enrichment in a silylated derivative of the deoxyribose moiety of the purine nucleosides was measured by gas chromatography/pyrolysis/isotope ratio-mass spectrometry (GC/P/IR-MS). Samples were analyzed on a Finnigan DELTA$^{PLUS}$ XP IRMS instrument (ThermoFisher, Bremen, Germany) fitted with a DB-5ms column (Agilent, Santa Clara, CA). The fraction of newly divided $CD5^+CD19^+$ cells, *f*, at each sampled time point was calculated from the

$^2H$ enrichment (atom percent excess, APE) value. This value represents the isotope enrichment above natural abundance of deuterium due to incorporation of $^2H_2O$ into newly synthesized DNA (into the deoxyribose moiety), divided by the time-averaged $^2H_2O$ exposure prior to each sampled time point over the duration of the preceding labeling period.

***Calculation of fractional birth and death rates from CLL labeling data and CLL cell counts***

*In vivo* labeling of proliferating CLL cells was carried out by individuals drinking small volumes of $^2H_2O$ each day to stably enrich the body water pool with $^2H_2O$, so that $^2H$ is incorporated into the DNA of cells that divide during the period of label exposure. The rate of cellular proliferation (or "birth rate") was estimated in two complementary ways: first, during the period of $^2H_2O$ exposure *in vivo*, based on the rate of $^2H$ incorporation into DNA of CLL cells; and, second, during the period after $^2H_2O$ had washed out of the body water pool, based on the dilution of previously $^2H$-labeled CLL cells by newly divided unlabeled cells. Specifically, in the pre-ibrutinib period, birth rate ($k_b$) was calculated from the fraction of newly proliferated cells (f) during weeks 0-8 of $^2H_2O$ incorporation (Figure 2B; averages of all patients shown) using a regression fit for results from serial time points based on a single pool monoexponential rise-to-plateau model ($f = 1 - e^{(-k_b * t)}$)(*2-4*). In the post-ibrutinib period, between 6-12 weeks after cessation of heavy water administration, fractional birth rate ($k_b$) was calculated from the decay rate of the proportion of cells containing $^2H$ label in DNA, again using a regression fit ($f = f_0 * e^{(-k_b * t)}$) to a monoexponential die-away model. The rates of change (R) in the pool size of

circulating CLL cells during the corresponding pre- and post-ibrutinib periods, or the net exponential growth rates, were calculated by a regression fit of the blood absolute lymphocyte count (ALC) ($ALC = ALC_0 * e^{(R*t)}$). In the post-ibrutinib period, the effect of any transient lymphocytosis on calculated birth and death rates was minimized by including in the exponential decay fit only the time points starting from the peak value of ALC measured for each individual after initiation of ibrutinib therapy and followed through the subsequent 10 weeks. All regression fits were performed using the Prism software package (Graph Pad, La Jolla, CA). Finally, death rates ($k_d$) in the pre- and post-ibrutinib periods were calculated as the difference between the measured birth rate and the net exponential growth rate in blood ALC ($k_d = k_b - R$). Negative values for $k_d$ were assigned a value of zero.

***Tissue volumetric analysis***

The volume of lymphoid tissues and the spleen was quantified by computed tomography (CT) scans prior to therapy, and at the time of the first follow-up visit during ibrutinib therapy. Lymphoid tissue volumes were calculated from CT scans using the following method: the 5 largest conglomerations of LNs as well as the spleen were identified by visual inspection of the cases by a radiologist. A contour was hand drawn around the center CT slice containing each conglomerate of nodes. The area of the contoured region was used to calculate an effective radius using the formula for the area of a circle. For the spleen, a coronal diameter was also obtained and averaged with the effective axial diameter. The spherical volume was then calculated based on the effective radius. The total number of CLL cells in tissue was derived from the sum of measured tissue volumes, assuming that the average volume of a CLL cell is 166fl, as described(*5*).

***Mathematical modeling and estimation of tissue death rates***

The dynamics of CLL cells during ibrutinib therapy can be modeled by ordinary differential equations, which describe the development of the CLL-cell populations over time. Denoting CLL cells in tissue compartments (spleen and LNs) by *x*, and CLL cells in the blood by *y*, the model is as follows(*5*):

$$\frac{dx}{dt} = -mx - d_1(x + c)$$
$$\frac{dy}{dt} = mx - d_2 y$$

In the tissue compartment, CLL cells are assumed to die with a rate $d_1$, and are further assumed to redistribute to the blood with a rate m. In the blood, CLL cells are assumed to die with a rate $d_2$. The parameter c describes phenomenologically the observation that the rate of decline of lymphocytes slows down over time and stabilizes around a steady state that can be higher than healthy levels. The reason behind this observation is not fully understood, so it is best to describe it in this phenomenological way. The model assumes the stabilization occurs in both the tissue and blood compartments. In accordance with prior preclinical data(*6-8*), lack of proliferation and tissue homing during ibrutinib therapy is assumed. This model was fit to the clinical data, and the best fit provided the parameter estimates. A comprehensive mathematical analysis of this mathematical model as well as issues related to fitting this model to clinical data are described in detail in(*5*). In order to uniquely estimate parameters, the model needs to be fit not only to the trended lymphocyte counts in the blood, but also to data that document the tumor burden in the tissues. In our previous cohort (*5*), we estimated tissue disease burden from radiological data that

measured the volumes of lymph nodes and the spleen before treatment and during therapy. Because the tissue is mostly made up of CLL cells at disease stages when treatment is initiated, and since we know the average volume of CLL cells, we can estimate the total number of cells in the tissue. In our previous work(*5*), the volumetric measurements were taken before treatment, and at two time points during treatment. At the first time point during treatment in study (*5*) (between 1-2 months after start of ibrutinib therapy), tissue sizes were still sufficiently large to estimate the number of tissue cells with reasonable accuracy. At the third time point, however, tissue sizes had already shrunk to near normal levels. At this stage, tissue size is unlikely to be a good indicator of the number of CLL cells in tissue. The volume of the tissue will stop shrinking, while the number of CLL cells is still on the decline. Hence, such relatively small tissue volumes cannot be used for our estimates.

In the current study, volumetric measurements were taken at two time points: before treatment, and about 80-90 days post treatment initiation. While the number of tissue cells before treatment could be reliably estimated from the tissue volumes, at the time point during ibrutinib therapy, the tissue volumes had already largely declined to near-normal levels, especially in those patients that responded relatively fast. Hence, the volumetric measurement during treatment could not be used to reliably estimate tissue tumor cell numbers in the current cohort.

Therefore, the model was fit to the trended lymphocyte counts, taking into account the volumetric measurements before ibrutinib therapy. We assumed that the total tissue tumor

burden before treatment was within a range of ± 10% of the number of CLL cells estimated from the volumetric analysis. As we have shown previously (*5*), in such a setting, i.e. without taking into account an estimate of tissue disease burden during treatment, the model can give rise to the same predicted blood lymphocyte dynamics under two alternative parameter combinations, making it difficult to uniquely determine a best fitting parameter combination. However, in our previous work (*5*), where tissue disease burden could be reliably estimated before and during treatment, the best fitting parameter combinations could be uniquely determined, and this showed that in all patients, $d_1 > d_2$, i.e. the death rate of CLL cells in tissue was found to be larger than that in blood. If we make the same assumption in the current cohort, then we can uniquely determine the parameter combination that best fits the data.

Thus, assuming that $d_1 > d_2$, the model was fit to the data as follows. As a first step, the model was simulated repeatedly for each patient with randomly chosen parameter values that were chosen from specified ranges. The sum of squared errors between observed and expected blood lymphocyte dynamics was calculated and recorded. This gave rise to "error landscapes" for each individual patient. Before discussing those, we specify the ranges from which parameter values were randomly chosen. $d_1 \in [0.001,20],\ d_2 \in [0.001,0.5],\ m \in [0.0001,0.1].$ The previously measured parameters (*5*) fall within these parameter ranges.

The parameter c was varied between 0 and an upper bound that was given by an estimated number of cells derived from the volumetric measurement during treatment. While the tissue volumes had already declined too much to reliably estimate the number of cells in

the tissue, this calculation can provide an upper bound of how many cells can be maximally left in the tissue. Finally, the total number of tissue CLL cells before treatment, and the number CLL cells in the blood before treatment were allowed to vary ± 10% from the data measurements.

We can plot the sum of squared errors between observed data and model predictions as a function of the tissue death rate $d_1$ (but varying all parameters simultaneously). This gives rise to what we call an "error landscape", and two different types of error landscapes were observed among the patients in the cohort. They are shown in Figure S1.

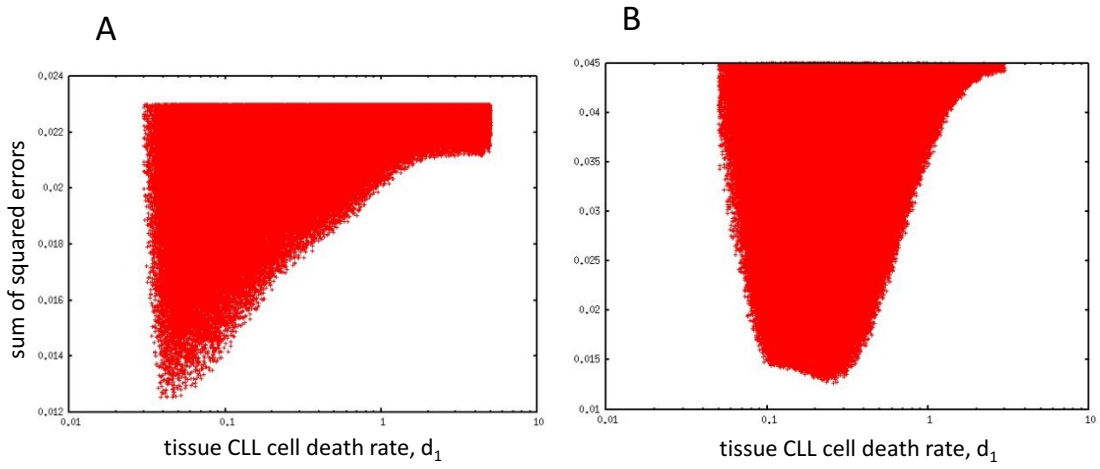


***Figure S1:*** *Sum of squared errors between model and data, assuming that $d_1>d_2$. All model parameters were varied randomly, and the error is plotted as a function of the tissue CLL cell death rate, $d_1$.* We refer to this as the "error landscape". *Each dot in the graph represents the outcome of one randomly chosen parameter combination. (A) A "slow responder" is characterized by having the smallest error for the smallest possible tissue cell death rate within the constraint $d_1>d_2$. (B) A "fast responder" is characterized by an intermediate value of $d_1$ that minimizes the error.*

The error landscape shown in Figure S1A is typical of a patient that shows treatment dynamics that are consistent with those observed in our previous study (*5*). That is, the

smallest error is observed for the smallest values of $d_1$, given that $d_1>d_2$. As the value of $d_1$ is increased, the error becomes larger (Figure S1A). The tissue death rate with the smallest error typically lies in the range between $d_1$=0.02-0.1 $d^{-1}$, which corresponds to an average CLL cell life-span of 10-50 days. Other patients in the current cohort are characterized by a different kind of error landscape, an example of which is shown in Figure S1B. In this case, an increase in $d_1$ first leads to a reduction in the error down to a minimum, beyond which the error then becomes larger again. The death rate $d_1$ with the smallest error in such patients typically lies above $d_1>0.1$, i.e. the average life-span of CLL cells is less than 10 days. While there is a value of $d_1$ where the error is the smallest, parameter combinations with somewhat larger errors can show model predictions that are visually still very good descriptions of the data. Given that data are noisy, it might thus be misleading to assume that the parameter combination with the smallest error is the true estimate for a given patient. Given that the tissue death rates, $d_1$, in this group of patients are significantly larger than in the first group, we adopted the following approach. We took the parameter values with the smallest error in our simulations and used them as an initial guess in a steepest decent model fitting algorithm, given by the software Berkeley Madonna (http://www.berkeleymadonna.com/). We then systematically reduced the initial guess for the tissue death rate, $d_1$, by using the decrement 0.01 and let this algorithm find a best fit, which is typically given by a local error minimum in the vicinity of the initial parameter guess. Once the value of $d_1$ fell below a threshold, such a local error minimum was not found anymore. Instead, significantly different parameter combinations were found and the error between model prediction and data became significantly lager. We took the lowest value of the tissue death rate $d_1$ that still yielded a local minimum with a reasonable fit and

assigned these parameters to the patient in question. This procedure yields the lowest tissue cell death rate that was still compatible with the data, and thus represents a conservative parameter estimate. We note that similar and perhaps slightly better fits could be obtained with higher tissue death rates in this group of patients. These values, however, corresponded to unrealistically high tissue cell death rates. Our quoted estimates should thus be considered as lower bounds. Even these lower bounds are clearly higher than the estimated death rate for the first group of patients. Note that the same procedure could be applied to the first patient group, yielding only a very small change in the parameter estimates.

Finally, note that the two different types of error landscapes can be used to classify patients into slow and fast responders. All patients in this cohort are characterized by error landscapes that clearly belong to either of the two groups presented in Figure S1. This indicates that there is something fundamentally different in these two groups. Even though some uncertainty exists about the magnitude of the tissue cell death rate in the fast responders, as discussed above, the error landscape indicates that they are indeed distinct from the slower responders. As discussed in the main text, genetic risk factors contribute to explaining this difference. Other, yet unknown factors, however, also seem to determine which response pattern is observed. A crucial factor might be whether patients have been previously treated with another form of therapy, or whether they are treatment naïve. Our previous cohort (*5*), in which we only observed the slow type of responders, was not treatment-naïve, while the current patient cohort was.

***Enrichments of $^2H_2O$ in plasma and appearance of $^2H$-labeled $CD19^+$ CLL cells in the PB***

The fractional enrichments of $^2H_2O$ in plasma, representing to the $^2H$-enrichment in body water, increased and reached a plateau during the first 4 weeks of labeling, while patients were drinking $^2H_2O$ on a daily basis (labeling period). The fraction of $^2H_2O$ in the body water pool increased from 0.05 ± 0.06% at baseline (week 0, mean ± SD, n=30) to 1.09 ± 0.21% after 2 weeks (n=29) and 1.11 ± 0.31% after 4 weeks (n=29, see Fig. 2A). Subsequently, after discontinuation of $^2H_2O$ intake, the fraction of $^2H_2O$ in the body water continuously declined and reached baseline levels by 10 -14 weeks after initiation of $^2H_2O$ intake or 6 – 10 weeks after discontinuation of $^2H_2O$ intake (washout period).

During the period of exposure to $^2H_2O$, the calculated fraction of $^2H$-labeled $CD19^+$ CLL cells increased from 0% at baseline (week 0) to 5.12 ± 4.08% after 2 weeks (n=26), to 10.57 ± 6.58% after 4 weeks (n=29), to 15.00 ± 7.31% after 6 weeks (n=28), and to 19.58 ± 8.13% after 8 weeks (n=28). Values generally stabilized after week 8, with 19.60 ± 6.55% $^2H$-labeled $CD5^+CD19^+$ cells measured after 10 weeks (n=29), and 20.31 ± 9.27% after 12 weeks (n=8, see Fig. 2B).

***Blood CLL cell death rates estimated by computational modeling***

We further investigated cell death rates during ibrutinib treatment based on a previously published mathematical methodology(*5*). This allowed us to obtain separate estimates for the tissue and blood compartments by fitting a two-compartment

mathematical model to data on trended lymphocyte counts in the blood as well as volumetric measurements of tissues (Fig. 4)(*5*). The model is summarized in Figure 5A, and explained in detail above. Select comparisons between model-predicted and observed trended lymphocyte counts are shown in Figure 5B, demonstrating good fits. Characteristically, with the end of the peak redistribution lymphocytosis, a rapid decline in blood leukemia cell counts is noted which later converts into a slower decline. The death rates estimated from this model correspond to the initial, rapid decline in cell numbers, which should reflect the death of the majority of CLL cells present at treatment initiation. Using this approach, we estimated the average death rate of CLL cells in the blood among all patients to be 2.34 ± 1.45% per day, which is higher than the estimate derived based on the decline slope of ALC in the blood. The reason for this difference is that this model assumes a continuous influx of CLL cells from the tissues to the blood, taking place during the initial weeks of therapy, even during the decline phase of lymphocytosis. The model estimates the magnitude of this influx, its decline over time, and thus incorporates this effect into the death rate estimates.

***Tissue CLL cell death rates estimated by computational modeling***

The estimated rates of tissue cell death varied considerably across patients (Fig. 5C). In another cohort of previously-treated CLL patients who received ibrutinib salvage therapy, we estimated that ~2.7% of cells died per day in tissue during therapy, which corresponds to an average CLL cell life-span of about 37 days(*5*). A subset of the current patient cohort has tissue cell death rates that are consistent with this previous estimate (Fig. 5C), with average CLL cell life-spans ranging between 10-50 days. In such patients, the dynamics in the blood exhibit a pronounced lymphocytosis phase, an example of which is

shown in Figure 5B (upper graph). However, other patients are characterized by estimated tissue cell death rates that are significantly higher, where tissue leukemia cells live on average only between 1-10 days during therapy (Fig. 5C). Such patients tend to have a shorter lymphocytosis phase in the blood and a faster decline in blood leukemia counts (Fig. 5B, lower graph). For each patient, simulation of the mathematical model with the estimated parameters outputs the tissue shrinkage dynamics over time, and the average time course of these computer simulations is plotted for patients with U-CLL and M-CLL in Figure 5D. The tissue is predicted to shrink faster in patients with U-CLL compared to those with M-CLL, and the predicted long-term plateau during treatment is lower for patients with U-CLL.

***Clinical responses***

At the time of analysis, median follow-up for all patients was 26 months and median treatment duration was 24 months. Twenty-seven of 30 patients (90%) continued on therapy without disease progression, 20 (67%) achieved partial remission, 9 (30%) complete remission, and 1 (3%) had stable disease, yielding an overall response rate (ORR) of 97%. Three patients came off study: one after 186 days due to suicide (ibrutinib-unrelated), and two after 575 and 658 days, respectively, due to toxicity (Grade 3 gastrointestinal hemorrhage and grade 2 joint aches and pains). Figure 3 (G and H) display the Kaplan Meier plots for progression-free survival (PFS) and overall survival (OS).

The clinical outcome also correlated with the CLL cell death rates in tissue. Patients with complete remission showed significantly faster estimated tissue cell death rates (33.88±8.19%) compared to patients with partial remission (16.37±11.91%), p=0.0018. No difference between these two groups of patients was observed for the estimated blood death

rate of CLL cells. The previous section reported that faster tissue cell death rates tended to occur in U-CLL compared to M-CLL patients. Consistent with this, 100% of the patients with complete remission displayed U-CLL, while this percentage was only 35% in patients with partial remission, a statistically significant difference ($p=0.0011$). Supporting this picture, we further found that the doubling time of the blood ALC before treatment was significantly faster in patients with complete remission (9.33±3.85 months) than in patients with partial remission (20.10±9.32 months), $p=0.0065$. These results underline the notion that more aggressive CLL responds better to ibrutinib therapy, presumably due to a higher dependence of the CLL cells on BCR signaling and BTK. The fact that ibrutinib therapy does not mobilize the majority of tissue CLL cells was already demonstrated by our earlier mathematical modeling that also was applied to this study(*5*). Based on volumetric changes in nodal sites and spleen, we estimated tissue disease burden and correlated this with PB disease burden during ibrutinib therapy. We calculated in a prior cohort of previously-treated patients that ibrutinib-induced redistribution of tissue-resident CLL cells into the PB accounted for only 23% of the tissue disease burden, while the remaining tissue CLL cells died before reaching the PB(*5*). These findings are recapitulated when this model is applied to this cohort of untreated patients. The clinical responses and response durations seen in this cohort are unsurprising and in line with previous reports about high activity of ibrutinib in untreated patients with CLL(*9-11*). Collectively, these data indicate that responses to ibrutinib are more complete and more durable when ibrutinib is used early in the course of the disease.

***Supplemental Table S1***

| ACC | Reasons to start treatment |
|---|---|
| 1 | progressive fatigue, lack of appetite, weight loss, recurrent infections |
| 2 | increasing fatigue, left upper quadrant pain, occasional night sweats |
| 3 | hyperleukocytosis, anemia, fatigue |
| 4 | anemia, short lymphocyte doubling time, fatigue |
| 5 | short lymphocyte doubling time |
| 6 | thrombocytopenia, fatigue |
| 7 | weight loss, night sweats, hyperleukocytosis |
| 8 | thrombocytopenia, splenomegaly |
| 9 | short lymphocytoe doubling time |
| 10 | progressive hyperleukocytosis, anemia, hypogammaglobulinemia, recurrent infections. |
| 11 | thombocytopenia, recurreent infections |
| 12 | anemia, thrombocytopenia, fatigue |
| 13 | anemia, thrombocytopenia, lymphadenopathy |
| 14 | severe fatigue |
| 15 | hyperleukocytosis, thrombocytopenia |
| 16 | anemia, thrombocytopenia, fatigue |
| 17 | hyperleukocytosis, hepatosplenomegaly |
| 18 | anemia, thrombocytopenia, splenomegaly |
| 19 | anemia |
| 20 | anemia, thrombocytopenia, fatigue |
| 21 | anemia, hyperleukocytosis |
| 22 | thombocytopenia |
| 23 | anemia, hyperleukocytosis |
| 24 | anemia, thrombocytopenia, splenomegaly |
| 25 | hyperleukocytosis, splenomegaly |
| 26 | thrombocytopenia, lymphadenopathy |
| 27 | anemia |
| 28 | anemia, thrombocytopenia, hepatosplenomegaly |
| 29 | hyperleukocytosis, splenomegaly |
| 30 | fatigue, thrombocytopenia |

***Supplemental figures (panels 1-30)***

Percent $^{2}H$ enrichment in the DNA of PB CLL cells from the CLL patients was measured and converted into a fraction (f) of newly divided cells as described in Methods. After starting ibrutinib therapy (labeled "Start drug" in the left upper panels) in the period after $^{2}H_2O$ has washed out of the body water pool, there is a stable plateau in the proportion of labeled CLL cells. The absence of dilution in f (the fraction of previously divided, labeled CLL cells) by newly divided, unlabeled CLL cells indicates an arrest of new CLL cell birth. Commentary on each individual's labeling and de-labeling patterns are included in the figures.

# Patient 1

- Net birth rate: 0.65% /day

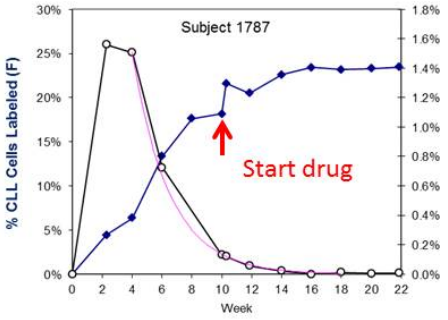


Clearance of WBC on Drug: Sub 1

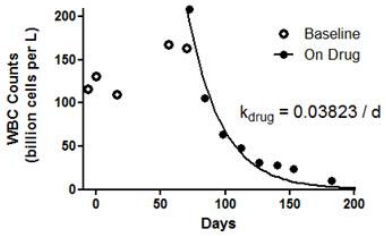


Asymptote Model
(label incorporation & disappearance rates)

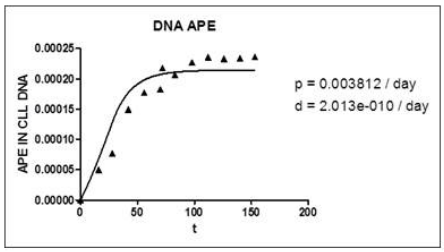


- 27% spike in WBC counts but label enrichment also spikes with the onset of drug.
  - Rules out proliferation, which would dilute label at low body water enrichments
  - Therefore, mobilization of a more highly enriched compartment
- Stable F with declining counts on drug
  - Lack of ongoing proliferation to dilute labeled cells
  - Unbiased clearance (death or sequestering) that exceeds the baseline turnover rate

# Patient 2

- Net birth rate: 0.58% /day

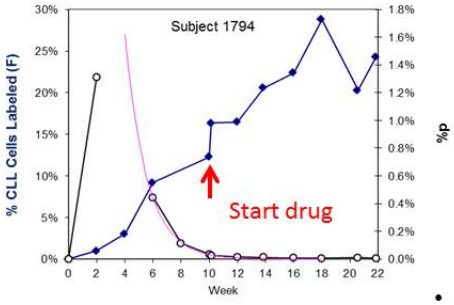


Clearance of WBC on Drug: Sub 2

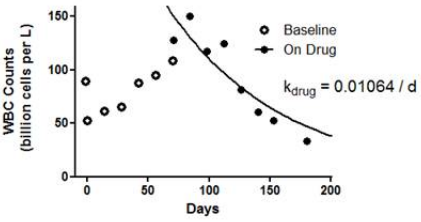


Asymptote Model
(label incorporation & disappearance rates)

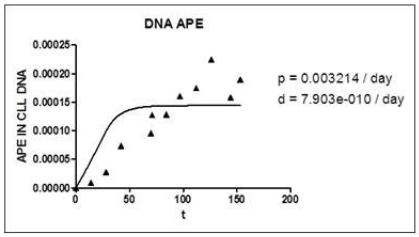


- Spike in WBC counts but label enrichment increases with the onset of drug
  - Rules out proliferation, which would dilute label at low body water enrichments
  - Increase in label enrichment after D2O is washed out indicates mobilization of a more enriched hidden compartment that persists.
- Increasing F with declining WBC counts
  - No ongoing proliferation to dilute labeled cells
  - Unbiased clearance (death or sequestering)
  - Delayed appearance of new cells

# Patient 3

- Net birth rate: 1.06% /day

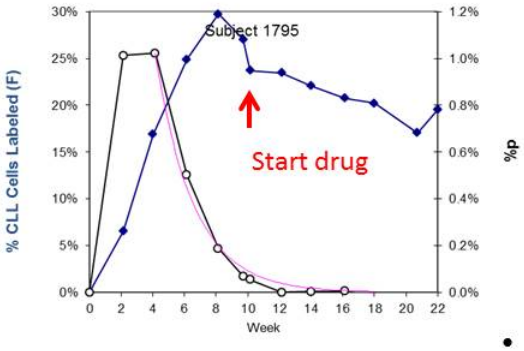


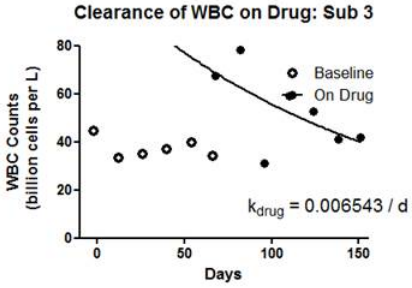


Asymptote Model
(label incorporation & disappearance rates)

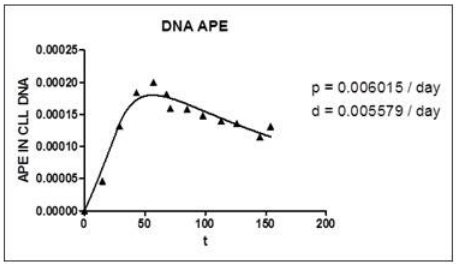


- Drug effect at week 10 induces an acute dilution of labeled cells in circulation.
- WBC Counts double with drug, while labeled cells dilute only 12%
  - Proliferation cannot account for acute increase in circulating cells
- Slow decline in F on drug indicates label dilution by proliferation.

# Patient 4

- Net birth rate: 0.83% /day

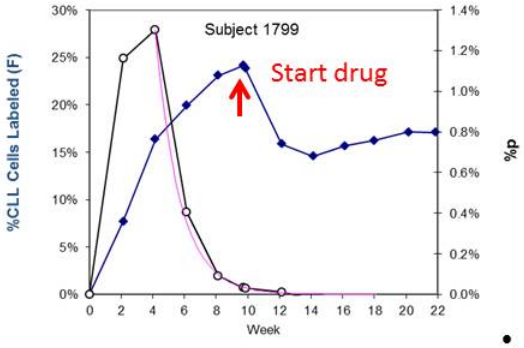


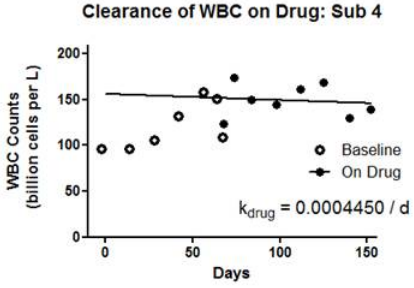


Asymptote Model
(label incorporation & disappearance rates)

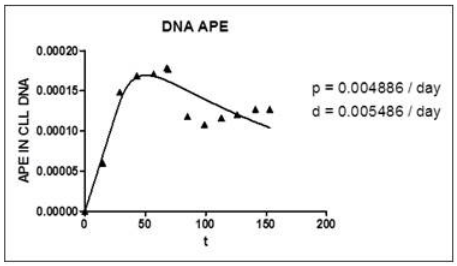


- Drug effect at week 10 induces an acute dilution of labeled cells in circulation, but no corresponding increase in WBC counts
- Both WBC Counts and fraction labeled cells (F) stay at a plateau value post treatment.
- WBC Counts did decrease after Wk 30

# Patient 5

- Net birth rate: 0.49% /day

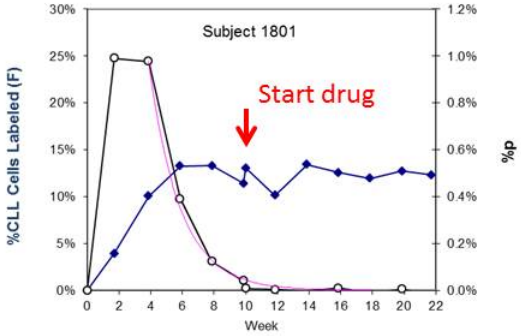


Asymptote Model
(label incorporation & disappearance rates)

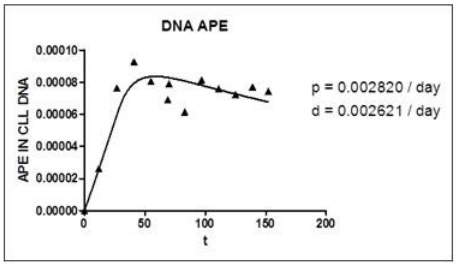


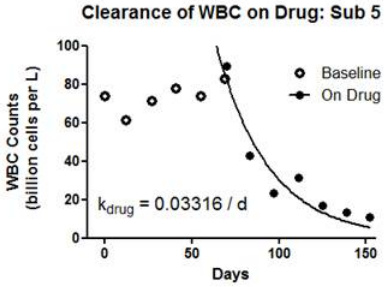


- Drug at week 10 does not have much effect on the fraction of labeled cells in circulation.
- WBC counts decrease sharply after an initial spike, but f stays constant
  - Little proliferation
  - Fast clearance

# Patient 6

- Net birth rate: 1.42 % /day

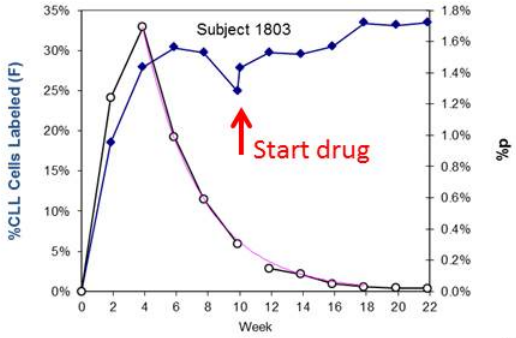


Asymptote Model
(label incorporation & disappearance rates)

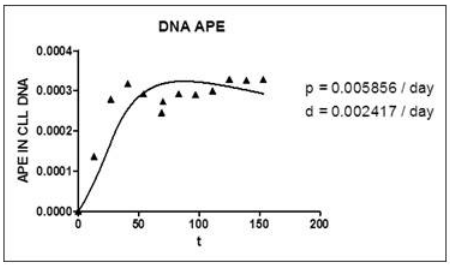


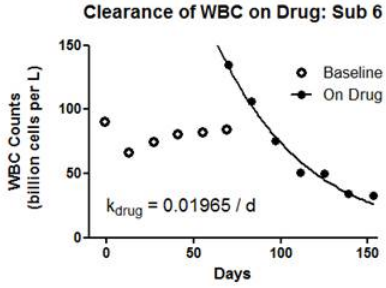


- Drug at week 10 interrupts a downward trend in % of labeled CLL cells, inducing an immediate spike which continues to creep upward.
- Slight BW at Wk 10 could not increase APE to the degree seen (e.g., spike in WBC counts not explained by proliferation)
- WBC counts decrease sharply after an initial spike, but f stays constant
  - No ongoing proliferation
  - Fast clearance

# Patient 7

- Net birth rate: 0.37 % /day

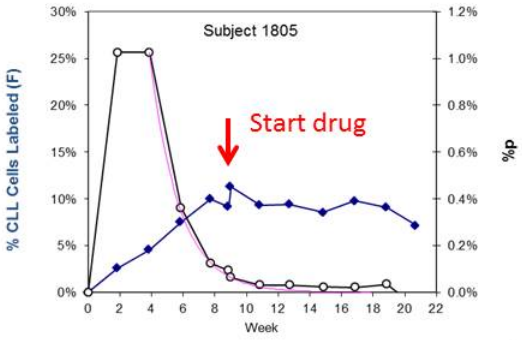


Asymptote Model
(label incorporation & disappearance rates)

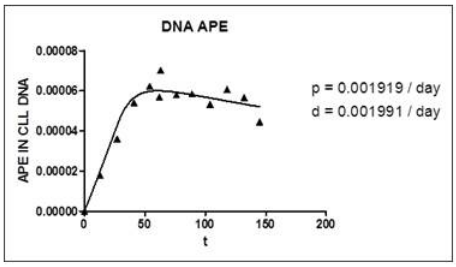


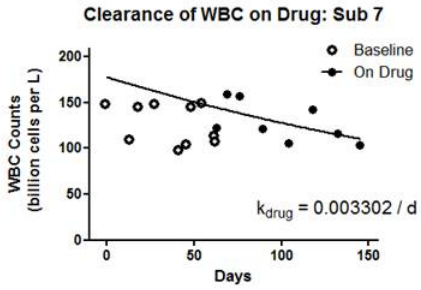


- Drug at week 9 does not appear to affect the % labeled cells or total WBC counts.
- WBC Counts do decrease at > 22 weeks.
- Slight proliferation is likely (F decreasing slightly, 0.2%/d)

# Patient 8

- Net birth rate: 0.32 % /day

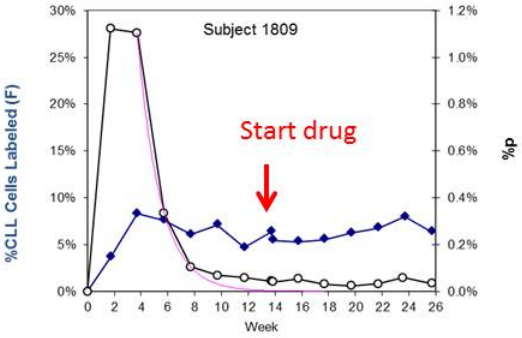


Asymptote Model
(label incorporation & disappearance rates)

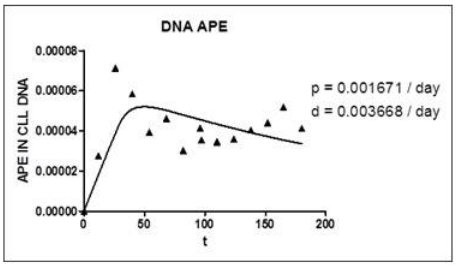


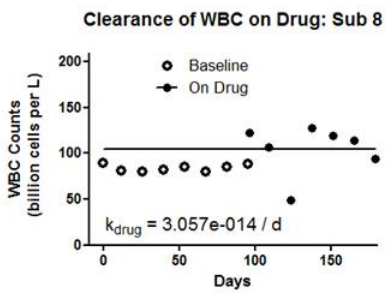


- Drug at week 14 does not appear to affect the % labeled cells or total WBC counts.
- WBC Counts did decrease at > 30 weeks.
- No proliferation is detected

# Patient 9

- Net birth rate: 0.61 % /day

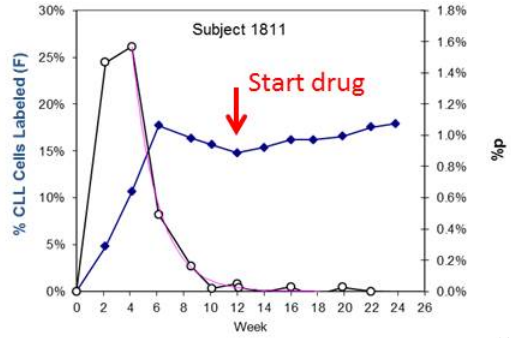


Asymptote Model
(label incorporation & disappearance rates)

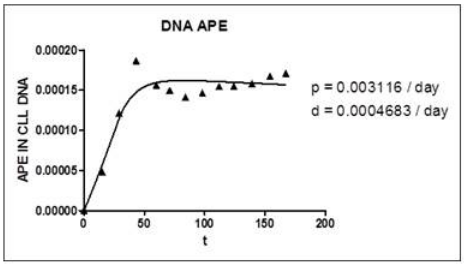


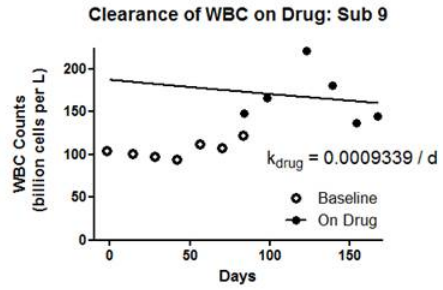


- Increase in WBC counts with drug, with no affect on %F indicates redistribution rather than proliferation
- Drug stabilized %F at plateau No proliferation is detected
- WBC Counts decreased at > Wk 30

# Patient 10

- Net birth rate: 0.34 % /day

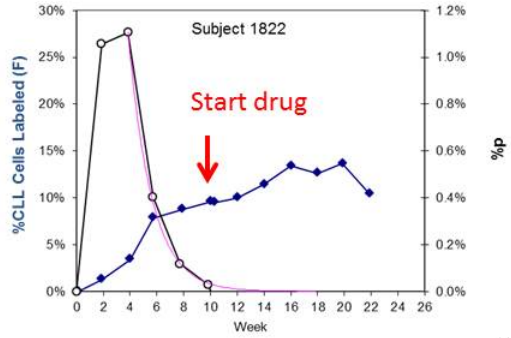


Asymptote Model
(label incorporation & disappearance rates)

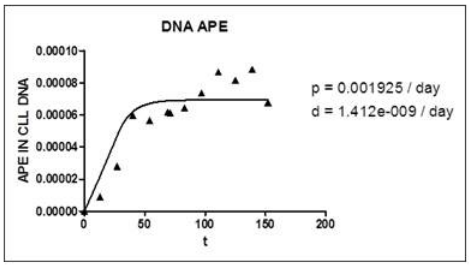


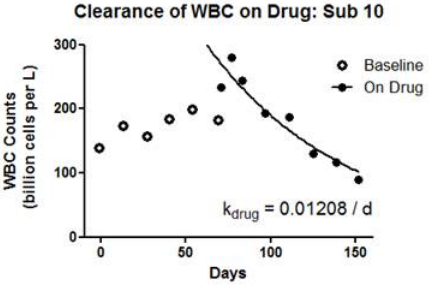


- Decrease in WBC counts with little or no change in % Cells Labeled
  - No evidence of proliferation with Drug
  - Inhibition of proliferation insufficient to explain fast clearance of WBC (also inducing death/ sequestration)

# Patient 11

- Net birth rate: 0.54 % /day

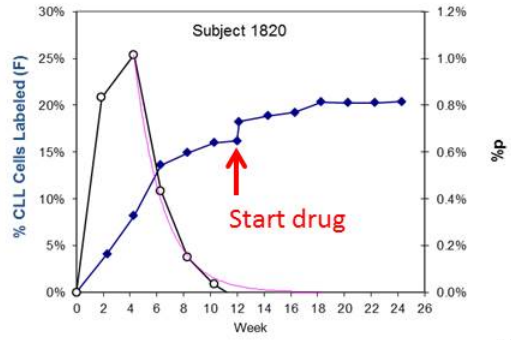


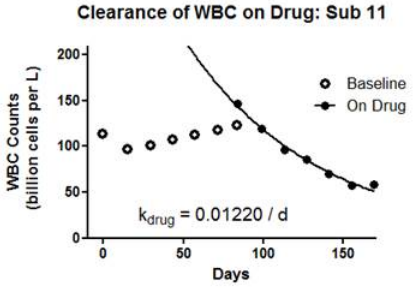


Asymptote Model
(label incorporation & disappearance rates)

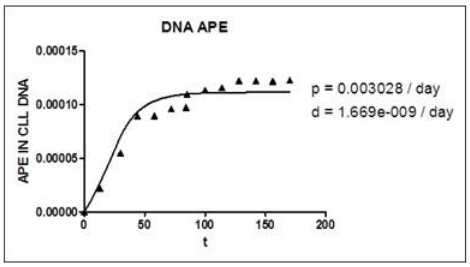


- Spike in F with drug due to redistribution rather than proliferation
- Decrease in WBC counts with little or no change in % Cells Labeled
  - No proliferation with Drug
  - Inhibition of proliferation insufficient to explain fast clearance of WBC, which also must induce unbiased death/ sequestration

# Patient 12 (drug holiday)

- Net birth rate: 1.4 % /day

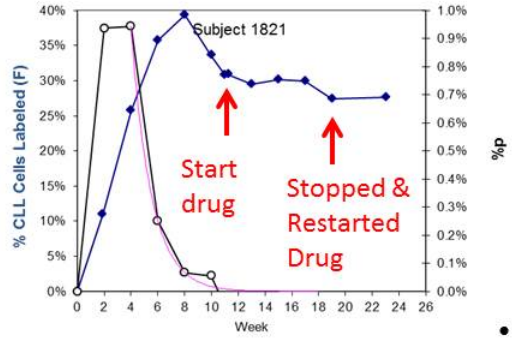


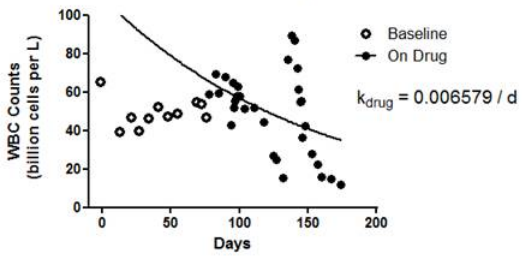


Asymptote Model
(label incorporation & disappearance rates)

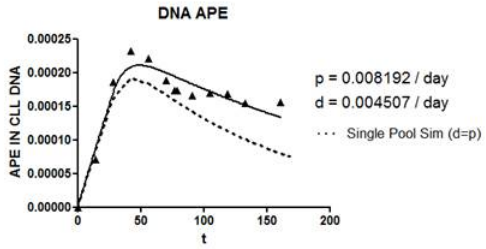


- Starting drug stabilized F
  - F trends down, even after drug, but not as fast as it's pre-dose trajectory
  - Label decay rate (d) is still less than label incorp rate (p)
- Stopping (5 days) then restarting drug had big effect on WBC counts, but not on F
  - Redistribution more likely than proliferation, but where are cells going when they leave the blood?

# Patient 13

- Net birth rate: 0.83 % /day

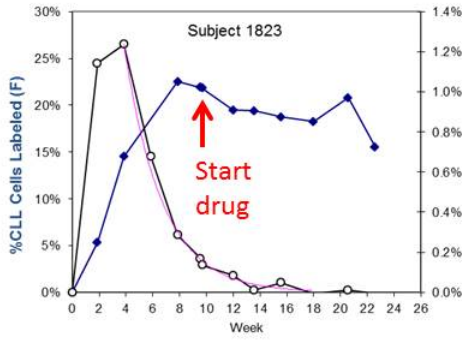


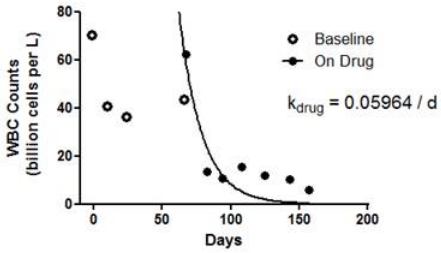


Asymptote Model
(label incorporation & disappearance rates)

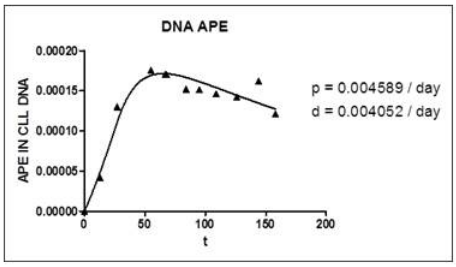


- Slow decay in F indicates a label disappearance rate of 0.4%/d (relatively high).
  - Indicative of ongoing proliferation or preferential loss of labeled cells even as WBC counts decline
- A unique phenotype
  - This was the only patient in this study whose enrichments fell on-drug (indicating ongoing prolideration) while exhibiting a rapid leukopenia response.

# Patient 14

- Net birth rate: 0.37 % /day

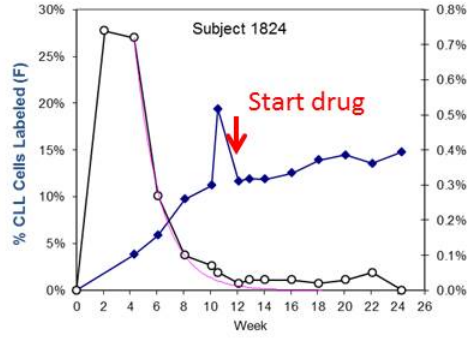


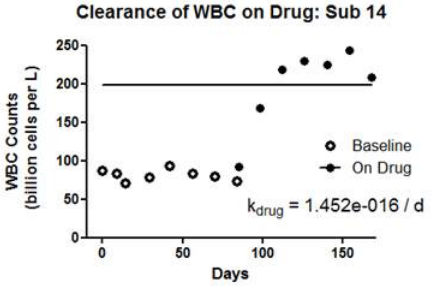


Asymptote Model
(label incorporation & disappearance rates)

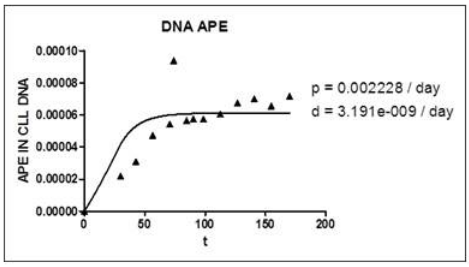


- Big spike in WBC Counts are not due to proliferation
  - Continued increase in F could not be due to ongoing proliferation, so lag ?
  - This subject eventually returns WBC counts to baseline (at 60 wks)
  - Would be interesting to analyze week 60 F.

# Patient 15

- Net birth rate: 0.62 % /day

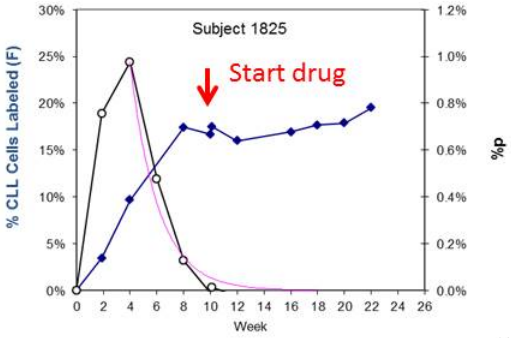


Asymptote Model
(label incorporation & disappearance rates)

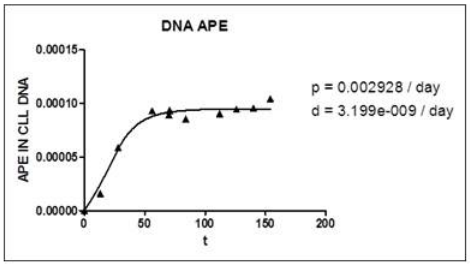


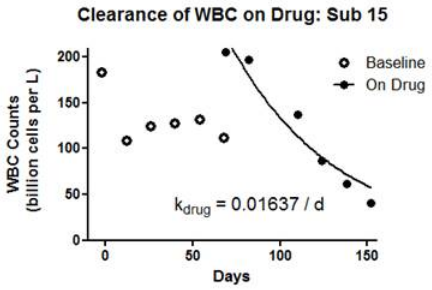


- Decrease in WBC counts with little or no change in % Cells Labeled
  - No evidence of proliferation with Drug
  - Inhibition of proliferation insufficient to explain fast clearance of WBC (also inducing death/ sequestration)

# Patient 16

- Net birth rate: 0.70 % /day

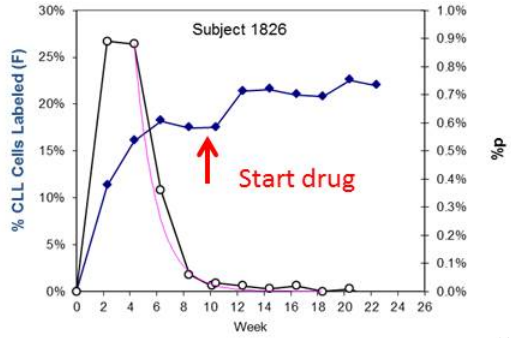


Asymptote Model
(label incorporation & disappearance rates)

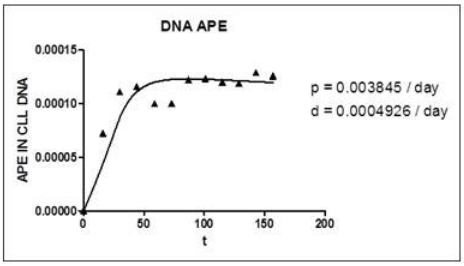


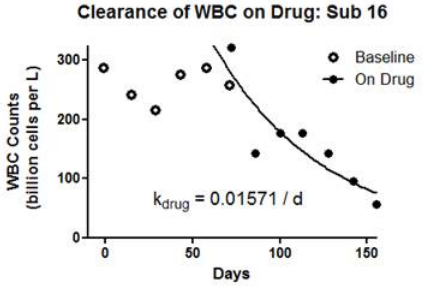


- Decrease in WBC counts with little or no change in % Cells Labeled
  - No evidence of proliferation with Drug
  - Inhibition of proliferation insufficient to explain fast clearance of WBC (also inducing death/ sequestration)

# Patient 17

- Net birth rate: 0.33 % /day

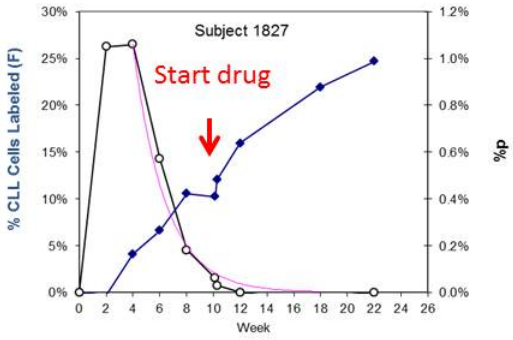


Asymptote Model
(label incorporation & disappearance rates)

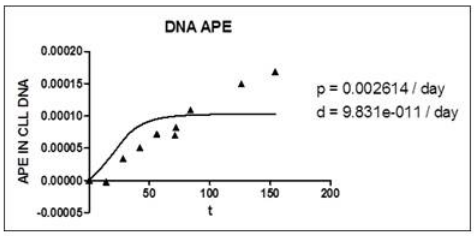


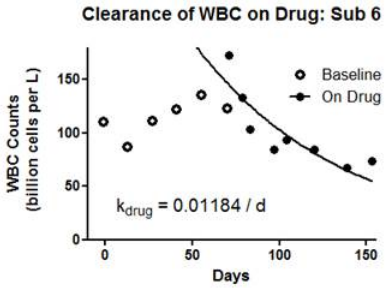


- Lag in this subject is evident
  - New CLL Cells have a delayed appearance into the blood stream even after drug therapy is started.

# Patient 18

- Net birth rate: 0.56 % /day

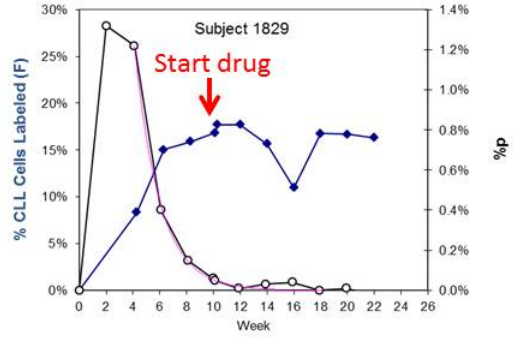


Asymptote Model
(label incorporation & disappearance rates)

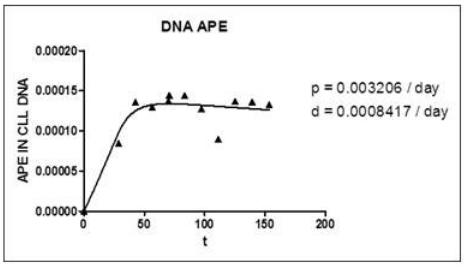


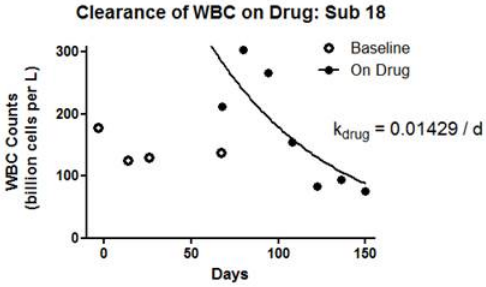


- Leukocytosis (2X) not caused by proliferation, but rather redistribution
- WBC counts decrease rapidly while F stays relatively level

# Patient 19

- Net birth rate: 0.78 % /day

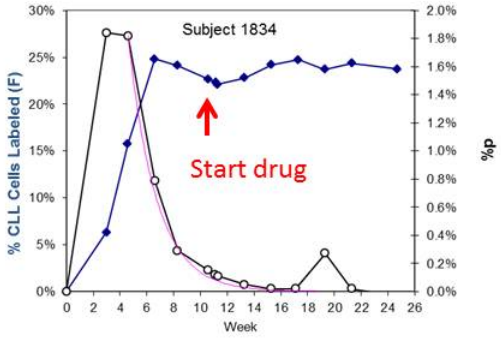


Asymptote Model
(label incorporation & disappearance rates)

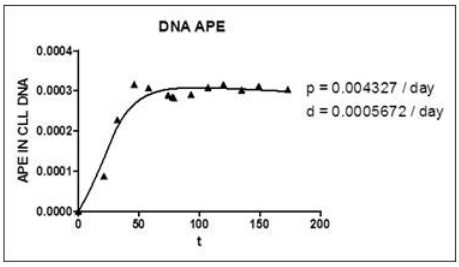


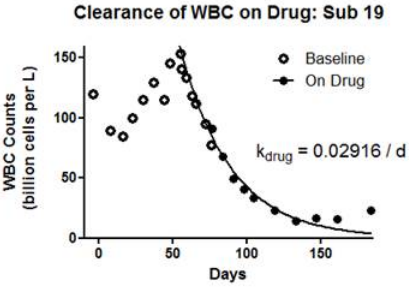


- No acute leukocytosis, and post-drug, the WBC clearance is rapid, while F stays relatively level (ie, no proliferation)

# Patient 20

- Net birth rate: 0.71 % /day

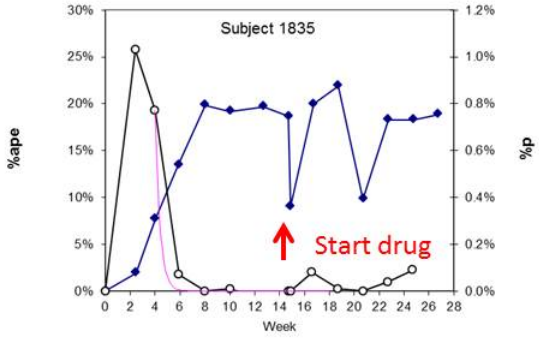


Asymptote Model
(label incorporation & disappearance rates)

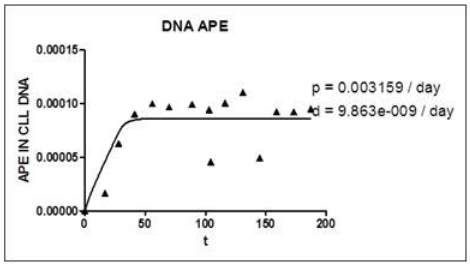


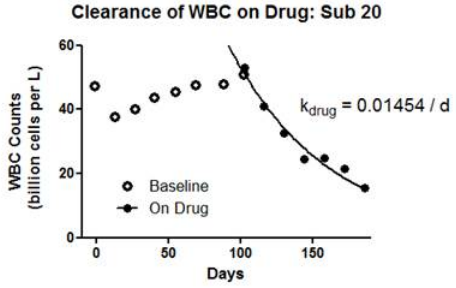


- The temporary decrease in CLL F when drug is started is difficult to reconcile with the lack of a measurable change in WBC counts

# Patient 21

- Net birth rate: 0.55 % /day

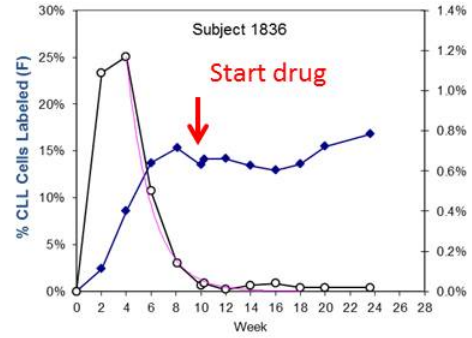


Asymptote Model
(label incorporation & disappearance rates)

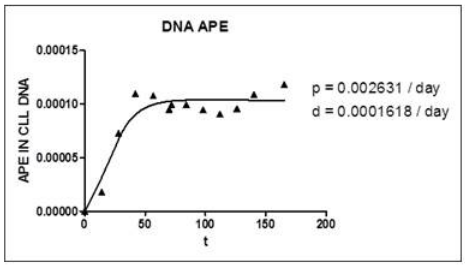


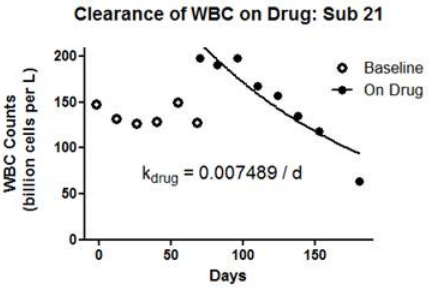


- No decrease in F during acute leukocytosis as would be expected from proliferation
- Stable F while WBC counts decrease, albeit relatively slowly.

# Patient 22

- Net birth rate: 0.74 % /day

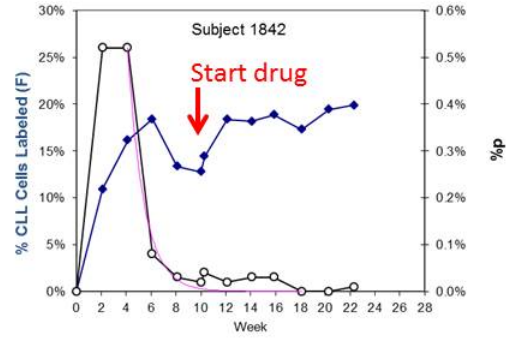


Asymptote Model
(label incorporation & disappearance rates)

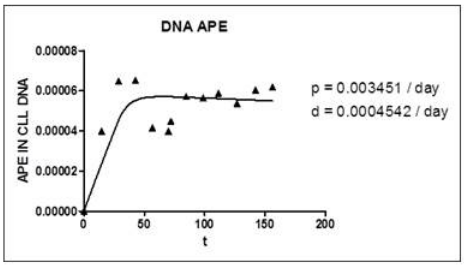


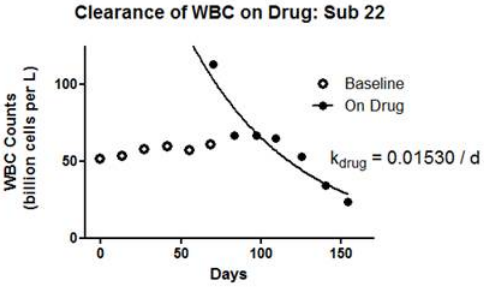


- Doubling in WBC counts with drug coincides with an increase in F, in the absence of D2O, indicative of redistribution from a more enriched compartment.
- Stable F while WBC counts decrease with chronic dosing

# Patient 23

- Net birth rate: 0.49 % /day

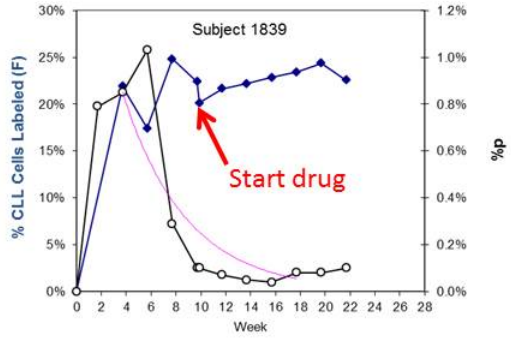


Asymptote Model
(label incorporation & disappearance rates)

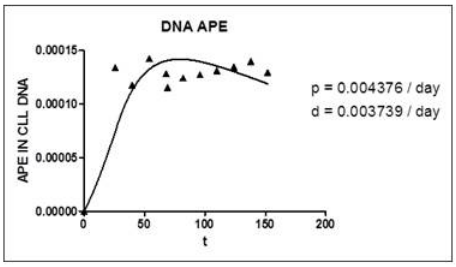


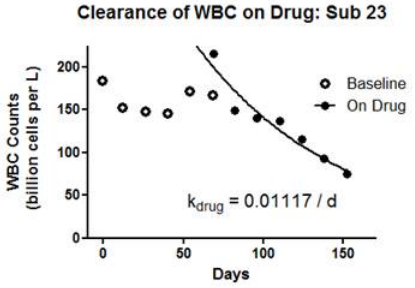


- 30% increase in WBC counts with drug could be partially attributed to proliferation (CLL enrichment decreased 10% concomittantly)
- Afterwards, stable F while WBC counts decrease with chronic dosing

# Patient 24

- Net birth rate: 0.85 % /day

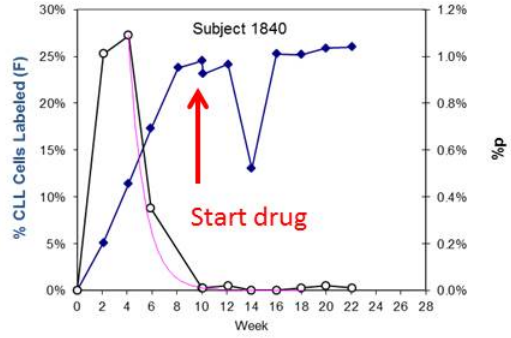


Asymptote Model
(label incorporation & disappearance rates)

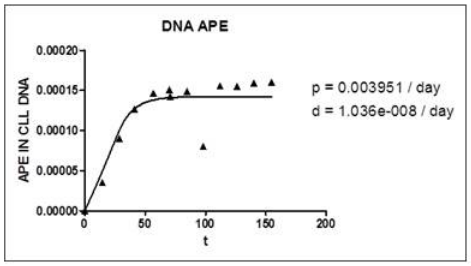


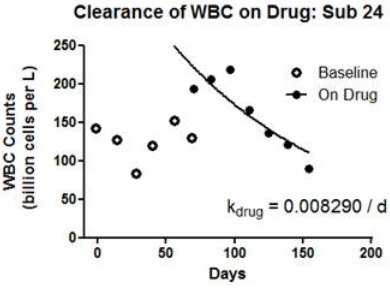


- 49% increase in WBC counts with drug coincides with a slight decrease in CLL enrichment decreased (6%)
- Afterwards, stable F while WBC counts decline to baseline (will continue to decline)

# Patient 25

- Net birth rate: 0.55 % /day

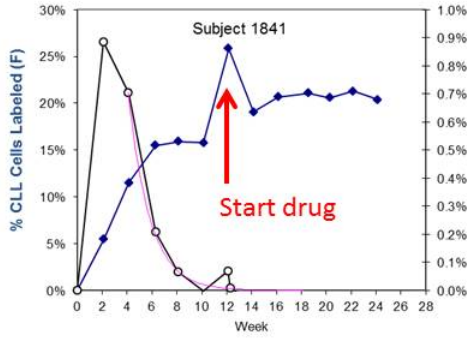


Asymptote Model
(label incorporation & disappearance rates)

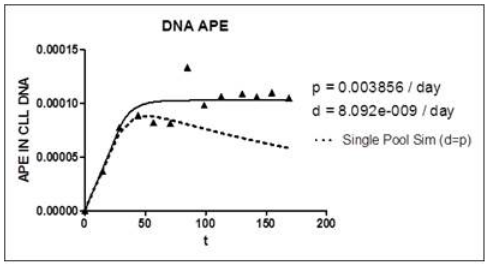


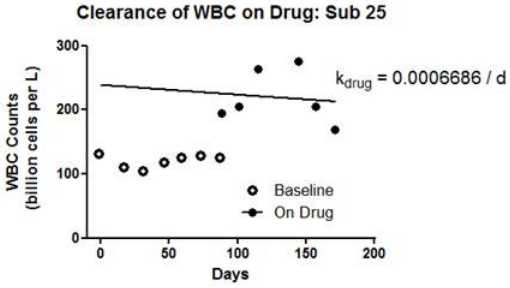


- 2X increases in WBC counts with drug coincides with a large increase in CLL enrichment, which could not be explained by proliferation
- Afterwards, stable F while WBC counts do not decline to baseline
- Counts decline after Week 30

# Patient 26

- Net birth rate: 0.56 % /day

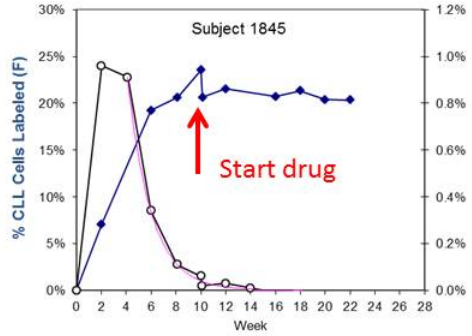


Asymptote Model
(label incorporation & disappearance rates)

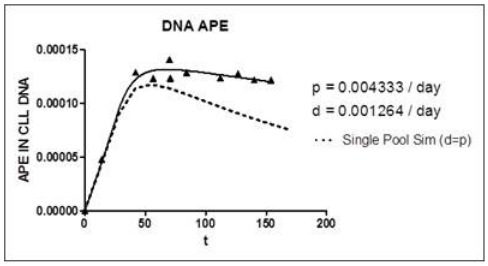


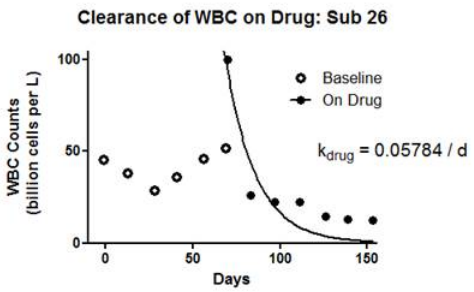


- 2X increases in WBC counts with drug has little dilution of F.
- Subsequent stable F while WBC counts decline indicates no proliferation, but increased death.

# Patient 27

- Net birth rate: 0.58 % /day

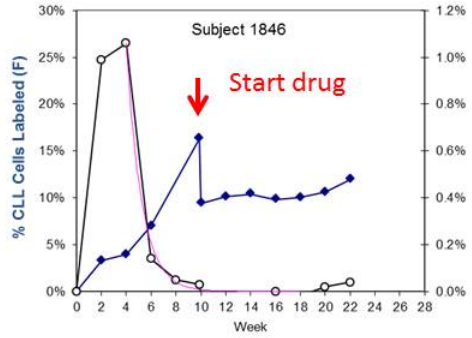


Asymptote Model
(label incorporation & disappearance rates)

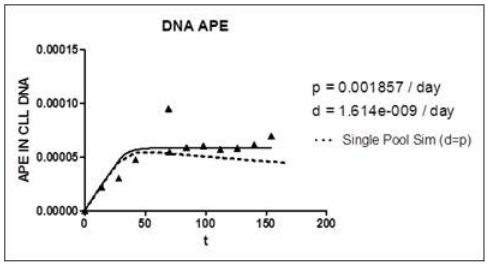


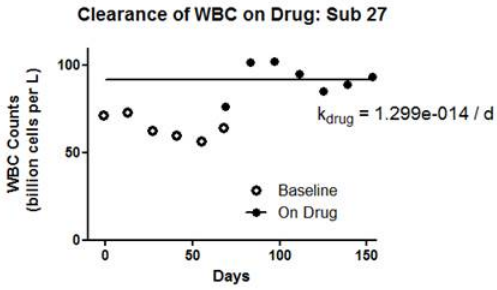


- This was the rare subject in which proliferation could explain the acute leukocytosis in circulation
- Subsequent stable F and WBC counts indicates no proliferation, but little death either.
- WBCs start to trend down at 33 weeks but only reaches baseline at 46 weeks.

# Patient 28

- Net birth rate: 0.62 % /day

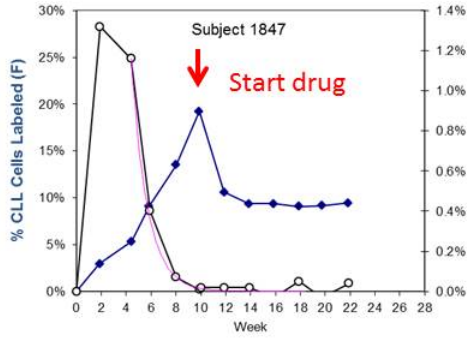


Asymptote Model
(label incorporation & disappearance rates)

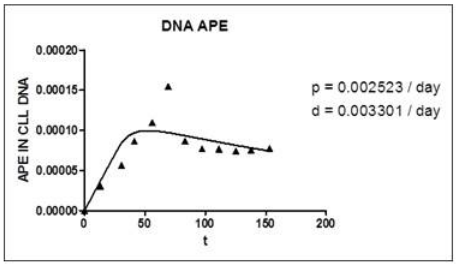


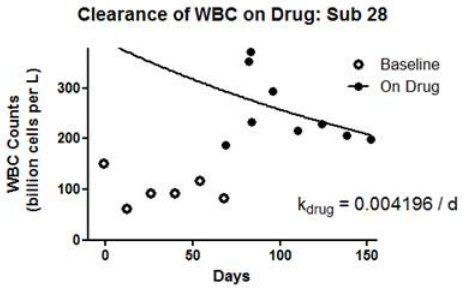


- This was the rare subject in which proliferation could explain the acute leukocytosis in circulation
- Subsequent stable F with elevated WBC counts indicates no proliferation, but little death either.
- WBCs starting to trend down and eventually declines below baseline by 33 wks

# Patient 29

- Net birth rate: 0.55 % /day

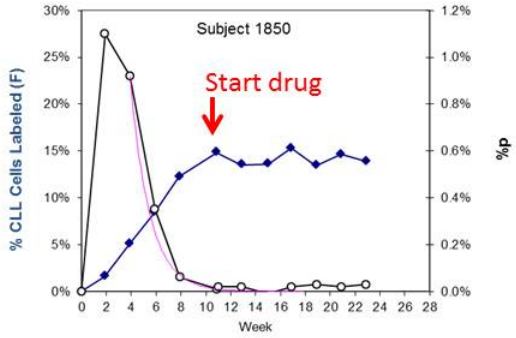


Asymptote Model
(label incorporation & disappearance rates)

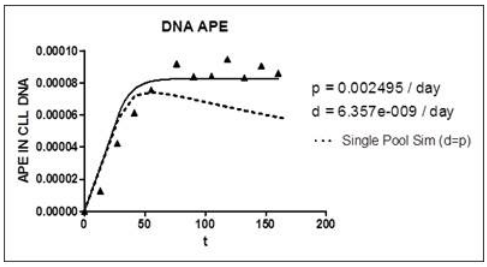


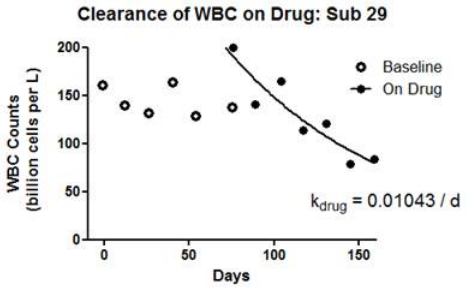


- Little acute leukocytosis, and on-drug, WBC clearance is consistent while F stays relatively level (i.e., no proliferation)

# Patient 30

- Net birth rate: 0.40 % /day

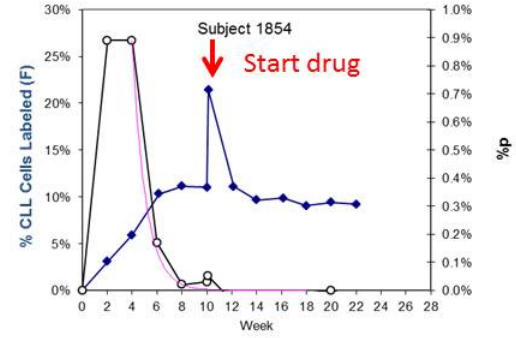


Asymptote Model
(label incorporation & disappearance rates)

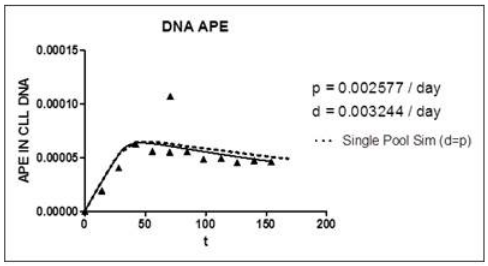


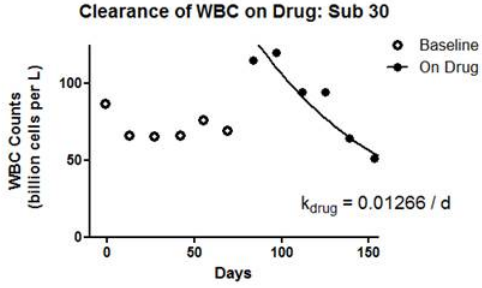


- 2X increases in WBC counts with drug coincides with a large increase in CLL enrichment, which could not be explained by proliferation
- Afterwards, stable F while WBC counts drop consistently

## References


1. B. T. Messmer, D. Messmer, S. L. Allen, J. E. Kolitz, P. Kudalkar, D. Cesar, E. J. Murphy, P. Koduru, M. Ferrarini, S. Zupo, G. Cutrona, R. N. Damle, T. Wasil, K. R. Rai, M. K. Hellerstein, N. Chiorazzi, In vivo measurements document the dynamic cellular kinetics of chronic lymphocytic leukemia B cells. *The Journal of clinical investigation* **115**, 755-764 (2005).
2. J. N. Voogt, M. Awada, E. J. Murphy, G. M. Hayes, R. Busch, M. K. Hellerstein, Measurement of very low rates of cell proliferation by heavy water labeling of DNA and gas chromatography/pyrolysis/isotope ratio-mass spectrometric analysis. *Nat Protoc* **2**, 3058-3062 (2007).
3. R. Busch, R. A. Neese, M. Awada, G. M. Hayes, M. K. Hellerstein, Measurement of cell proliferation by heavy water labeling. *Nat Protoc* **2**, 3045-3057 (2007).
4. R. A. Neese, L. M. Misell, S. Turner, A. Chu, J. Kim, D. Cesar, R. Hoh, F. Antelo, A. Strawford, J. M. McCune, M. Christiansen, M. K. Hellerstein, Measurement in vivo of proliferation rates of slow turnover cells by 2H2O labeling of the deoxyribose moiety of DNA. *Proceedings of the National Academy of Sciences of the United States of America* **99**, 15345-15350 (2002).
5. D. Wodarz, N. Garg, N. L. Komarova, O. Benjamini, M. J. Keating, W. G. Wierda, H. Kantarjian, D. James, S. O'Brien, J. A. Burger, Kinetics of CLL cells in tissues and blood during therapy with the BTK inhibitor ibrutinib. *Blood* **123**, 4132-4135 (2014).
6. S. E. Herman, A. L. Gordon, E. Hertlein, A. Ramanunni, X. Zhang, S. Jaglowski, J. Flynn, J. Jones, K. A. Blum, J. J. Buggy, A. Hamdy, A. J. Johnson, J. C. Byrd, Bruton tyrosine kinase represents a promising therapeutic target for treatment of chronic lymphocytic leukemia and is effectively targeted by PCI-32765. *Blood* **117**, 6287-6296 (2011).
7. S. Ponader, S. S. Chen, J. J. Buggy, K. Balakrishnan, V. Gandhi, W. G. Wierda, M. J. Keating, S. O'Brien, N. Chiorazzi, J. A. Burger, The Bruton tyrosine kinase inhibitor PCI-32765 thwarts chronic lymphocytic leukemia cell survival and tissue homing in vitro and in vivo. *Blood* **119**, 1182-1189 (2012).
8. S. S. Chen, B. Y. Chang, S. Chang, T. Tong, S. Ham, B. A. Sherry, J. A. Burger, K. R. Rai, N. Chiorazzi, Btk inhibition results in impaired CXCR4 chemokine receptor surface expression, signaling and function in chronic lymphocytic leukemia. *Leukemia* **in press**, (2015).
9. S. O'Brien, R. R. Furman, S. E. Coutre, J. P. Sharman, J. A. Burger, K. A. Blum, B. Grant, D. A. Richards, M. Coleman, W. G. Wierda, J. A. Jones, W. Zhao, N. A. Heerema, A. J. Johnson, R. Izumi, A. Hamdy, B. Y. Chang, T. Graef, F. Clow, J. J. Buggy, D. F. James, J. C. Byrd, Ibrutinib as initial therapy for elderly patients with chronic lymphocytic leukaemia or small lymphocytic lymphoma: an open-label, multicentre, phase 1b/2 trial. *Lancet Oncol* **15**, 48-58 (2014).
10. J. C. Byrd, R. R. Furman, S. E. Coutre, J. A. Burger, K. A. Blum, M. Coleman, W. G. Wierda, J. A. Jones, W. Zhao, N. A. Heerema, A. J. Johnson, Y. Shaw, E. Bilotti, C. Zhou, D. F. James, S. O'Brien, Three-year follow-up of treatment-naive and previously treated patients with CLL and SLL receiving single-agent ibrutinib. *Blood* **125**, 2497-2506 (2015).

11. J. A. Burger, A. Tedeschi, P. M. Barr, T. Robak, C. Owen, P. Ghia, O. Bairey, P. Hillmen, N. L. Bartlett, J. Li, D. Simpson, S. Grosicki, S. Devereux, H. McCarthy, S. Coutre, H. Quach, G. Gaidano, Z. Maslyak, D. A. Stevens, A. Janssens, F. Offner, J. Mayer, M. O'Dwyer, A. Hellmann, A. Schuh, T. Siddiqi, A. Polliack, C. S. Tam, D. Suri, M. Cheng, F. Clow, L. Styles, D. F. James, T. J. Kipps, R.-. Investigators, Ibrutinib as Initial Therapy for Patients with Chronic Lymphocytic Leukemia. *The New England journal of medicine* **373**, 2425-2437 (2015).